Hybrid Nanocluster Plasmonic Resonator for Immunological Detection of Hepatitis B Virus

Mohamed Shehata Draz,[†,‡] Binbin Amanda Fang,[§,⊥] Lanjuan Li,[‡] Zhi Chen,[‡] Yingjie Wang,[‡] Yuhong Xu,[†,¶] Jun Yang,[†] Kevin Killeen,[#] and Fanqing Frank Chen[†,§,*]

[†]Zhejiang-California International Nanosystems Institute, Zhejiang University, Hangzhou, Zhejiang 310029, China, [‡]State Key Laboratory for Infectious Diseases Diagnosis and Treatment, the First Affiliated Hospital, School of Medicine, Zhejiang University, Hangzhou 310003, China, [§]Life Sciences Division, Lawrence Berkeley National Laboratory, Mailstop 977, 1 Cyclotron Road, Berkeley, California 94720, United States , [⊥]Life Sciences College, Fudan University, Shanghai 200433, PR China, [¶]School of Pharmacy, Shanghai Jiao Tong University, Shanghai 200240, PR China, and [#]Agilent Laboratory, 5301 Stevens Creek Boulevard, Santa Clara, California 95051-7201, United States

ABSTRACT

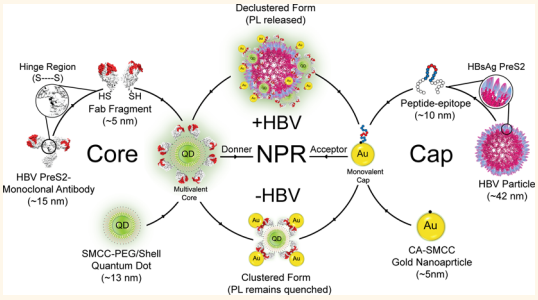

Approximately 88% of the world population lives in regions with intermediate to high incidence of Hepatitis B virus (HBV), yet current serological and DNA-based detection methods have limited sensitivity and convenience. Here, we describe a preassembled plasmonic resonance nanocluster for HBV detection. The gold nanoparticle acceptors (AuNPs), with HBV surface antigen (HBsAg) epitope, and quantum dot (QD) donors with Fab antibody, are assembled into an immuno-mediated 3D-oriented complex with enhanced energy transfer and fluorescence quenching. The coherent plasmonic resonance between Au and QD nanoparticles is exploited to achieve improved donor—acceptor resonance within the nanocluster, which in the presence of HBV viral particles is disassembled in a highly specific manner. The nanocluster provides high detection specificity and sensitivity of HBV, with a sensitivity limit down to 1—100 viral particles per microliter and to attomolar levels of HBsAg. This general platform could be used to establish multiplex diagnostic assays for a variety of other microbial pathogens.

KEYWORDS: nanocluster · plasmonic · gold nanoparticle · quantum dots · Hepatitis B virus · biosensing

Recent advances in nanotechnology present exciting opportunities to create interclustering hybrid nanostructures with broadly tunable and enhanced properties. Successful use of noble metals, especially gold, has inspired a great body of research efforts on photonic nanostructures.[1] Gold nanoparticles (AuNPs) with characteristic surface plasmon resonance (SPR) were reported to drive intrinsic emission enhancement or photoquenching effects when interacting with photon emitters in the proximity.[2−5] These nanoscale distance-based plasmonic effects have guided increasing development for the integration of AuNPs into various nanoscale structures. On the other hand, the inherent optical properties of quantum dots (QDs), such as high quantum yield, size- and composition-tunable emission, broad excitation range, narrow and symmetric emission spectra, and excellent photostability, have enabled them to be ideal companions for AuNPs in fabrication of potent hybrid photonic nanostructures.[6−15] A plasmon-mediated nanomaterial surface energy transfer (NSET) mechanism analogous to fluorescence resonance energy transfer (FRET) was described in such hybrid nanostructures.[15,16] Au—QD as a pair of oscillating dipoles undergoes long-range dipole—dipole coupling, and the excitonic energy of QDs is known to be resonantly funneled and quenched into the plasmon of AuNPs. Following the concept of FRET, the energy transfer between QDs and AuNPs can be expressed in eq 1, which relates the resonance energy transfer efficiency E, to the Förster distance R_0, the Au—QD interdistance r, and the n number of Au-acceptors interacting with a single QD-donor; where the Förster distance is the distance at which the energy transfer is equal to 50%.[9,13,15]

$$E = \frac{R_0^6}{nR_0^6 + r^6} \quad (1)$$

The excited surface plasmons E_s are dependent on the strength of the applied electrical

* Address correspondence to f_chen@lbl.gov.

Received for review January 9, 2012 and accepted August 20, 2012.

Published online August 31, 2012
10.1021/nn3034056

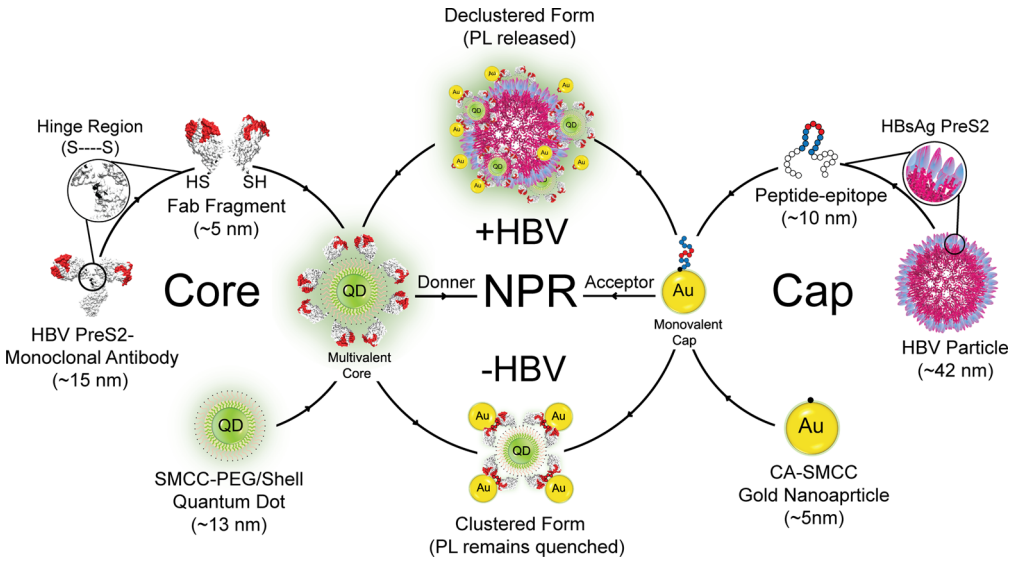

Figure 1. Schematic of HBV NPR complex. HBV NPR complex comprises two main conjugates of core conjugate (Core, left panel) and capping conjugate (Cap, right panel). Fab fragments were generated from monoclonal antibodies against HBV preS2 (HBV preS2 mAb) by cleavage followed by reduction of its hinge region disulfide bond (cysteine residues, the target of proteolytic cleavage and reduction reaction, are in black color). Peptide epitope corresponding in sequence to HBV preS2 antigen and specifically recognized by the Fabs was synthesized, and additionally modified with synthetic C-terminal cysteine. Through the thiol-amine cross-linking chemistry using the SMCC cross-linker, the prepared Fabs and peptide epitope were directionally conjugated to quantum dots (QDs) and gold nanoparticles (AuNPs) to prepare multivalent Cores and monovalent Caps, respectively. Because of the affinity interaction between Fab fragments and its specific peptide epitope, the Caps (acceptor) and Core (donner, green glow) conjugates assemble together resulting in AuNPs plasmonically resonance-quenching QDs emission (central panel). In the presence of HBV, the NPR complex is disassembled; the capping and core conjugates declustered, and PL signal reemerges to allow virus detection (high green glow, upper central panel). In the absence of HBV, the NPR complex of caps−core conjugates remains clustered, allowing the plasmonic resonance of AuNP Caps to quench the photoluminescence (PL) of the QD Core (fainter green glow, bottom central panel). HBV capsid and antibody structures are modification and adaptation of data from the Protein Data Bank (HBV, 1QGT; antibody, 1IGT).

field E_0, and the induced (dipole) field in the particle. For a spherical particle with radius r_m, and dielectric constant ε, placed in a layer with dielectric constant ε_1, the overall field gain (G) of plasmonics can be represented as[17]

$$G(\omega) = \frac{E_s(\omega)}{E_0(\omega)} \approx 1 + \frac{\varepsilon(\omega) - \varepsilon_1}{\varepsilon(\omega) + 2\varepsilon_1}\left(\frac{r_m}{r + r_m}\right)^3 \quad (2)$$

AuNPs surface plasmons were documented to attain energy-transfer distance up to 100 nm and by coupling with the QD-excitons this achieved enhancements beyond the limitations of traditional FRET.[18,19] We postulate that improvement and optimization of Au−QD interclustering and spatial arrangement will result in augmented plasmonic interaction, affording enhanced energy transfer with a minimal background interference, which will in turn significantly broaden the potential applications of hybrid Au−QD nanoplasmonics. The key is to control the interclustering parameters such as internanoparticle distance, spectral overlap, spatial orientation, and acceptor−donor ratio, so as to permit an efficient energy transfer without affecting the achievable sensitivity to perturbation of plasmonic resonance.[4,7−15] Several studies have successfully suggested that Au−QD hybrid clusters are superior building blocks for plasmonic sensing nanphotonics. So far, fluorescence quenching-based schemes have been established for the detection of heavy metal ions,[7] enzyme activity,[8,9] blood glucose level,[10] DNA,[11,12] protein glycosylation,[13,14] and more recently for the detection of prion protein.[15] Yet no previous effort has been successful in applying plasmonic resonance quenching to microbe detection. Virus and bacteria are orders of magnitude larger than small molecules and macromolecule complexes; their large sizes impact directly the distance-dependent resonance mechanism of NSET, leading to poor plasmonic resonance yield and imposing a challenge to an efficient detection of microbes. Here, we circumvent this issue with a novel high efficiency design, which will be the primary development focus in this report.

RESULTS AND DISCUSSION

We synthesized a preassembled plasmonic resonant nanocluster complex for HBV sensing, termed here "HBV nanocluster plasmonic resonator complex" (abbreviation: HBV NPR complex). It is a nanocluster composed of multiple capping nanoparticle conjugates and a single core nanoparticle conjugate (bottom of central panel, Figure 1). The peptide epitope, corresponding in sequence to HBV surface antigen preS2 (upper of right panel, Figure 1 and Supporting Information, Figure S1), and the Fab fragments targeting the epitope (derived from monoclonal antibody against

Figure 2. Schematic of nanocluster Caps preparation. AuNPs stabilized with citrate (negative ions) were first modified with cysteamine hydrochloride (CA) in the presence of Tween-20 (gray layer), and then 1-thioglycerol (TG) (green layer) was added. Using SMCC, C-terminal cysteine modified epitope peptides were coupled to particles (see Methods). The images show that the color does not change and no turbidity is visible (indicating that stability of AuNPs was maintained and there was no precipitation) throughout the preparation reactions.

HBV preS2 surface antigen, upper of left panel, Figure 1) have been used to mediate the preassembly of the Cap−Core nanocluster. The synthetic peptide was conjugated to AuNPs to prepare the nanocluster capping conjugates ("Caps", right panel of Figure 1), while the Fab fragments were covalently linked to amine-derivatized, polyethylene glycol−coated (PEG-coated) QDs to prepare the nanocluster core conjugates ("Core", left panel of Figure 1). When the core conjugates are added to the capping conjugates, as a result of the affinity interaction between a Fab fragment and its specific peptide epitope, the two conjugates assemble together with well-controlled spatial distance, orientation, and molar ratio, resulting in AuNPs plasmonic resonance quenched QDs emission (bottom of center panel, Figure 1). Upon exposure to HBV, the multiple copies of HBV viral surface protein preS2 competitively displace the epitope-carrying Caps bound on the Fab-carrying Core, causing disassembly of the HBV NPR complex in a highly specific manner (upper of center panel, Figure 1). The disassembly could be precisely measured by the fluorescence of the Core component with reduced association with the Cap component, which relieves the quenching of the QD emission by the gold nanoparticles.

In the nanocluster, the capping conjugates are AuNP monofunctionalized with a single preS2 peptide epitope, and were prepared as illustrated in Figure 2. Transmission electron microscopy (TEM) and the corresponding size distribution histogram show that the synthesized Au nanoparticles are spherical in shape with an average diameter of 5.5 ± 1.382 nm (Figure 3a, i and ii), confirmed by hydrodynamic sizing (Supporting Information, Figure S2) and HR-TEM (Figure S3). Acceptable monodispersity and stability were inferred from the ultraviolet−visible (UV−vis) spectrum with a strong and narrow surface plasmon absorption peak at 519 nm, dynamic light scattering (DLS) polydispersity index (PdI) value of 0.227 ± 0.124, and −30.533 ± 6.322 mV zeta potential value (Figure 3a,iii). The assessment of Au nanoparticles surface modification and peptide conjugation by UV−vis, Fourier transform infrared (FT-IR), and energy dispersive X-ray spectroscopy (EDX) techniques is presented in Figure 3b. A slight red shift to 521 nm is observed by UV−vis absorption analysis after the addition of cysteamine (CA), and to 525 nm

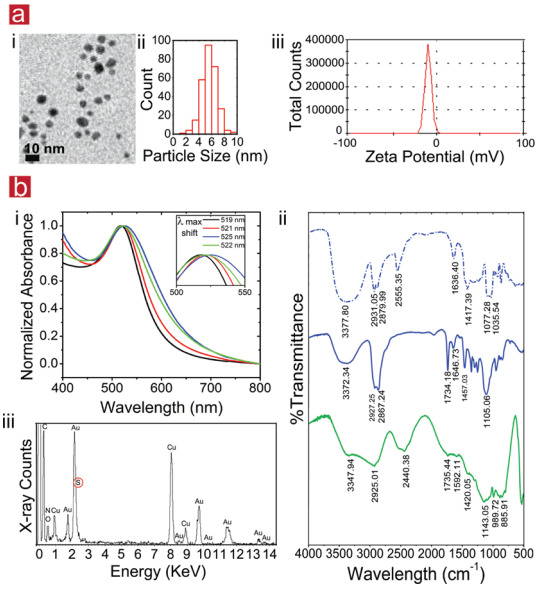

Figure 3. Nanocluster Caps preparation and characterization. (a) AuNPs characterization: (i) TEM image; (ii) particle size distribution histogram; (iii) zeta potential distribution spectrum. (b) AuNPs surface modification and peptide conjugation: (i) UV−vis absorption spectra of citrate (black), cysteamine (CA) (red), cysteamine+1-thioglycerol (CA+TG) (blue) and peptide (green) conjugated AuNPs. The inset indicates λ_{max} peak wavelength shift; (ii) FT-IR spectra of pure TG (dashed blue), CA+TG (blue) and CA+TG+ peptide (green) modified AuNPs, indicating the success of peptide conjugation onto the AuNP surface; (iii) EDX spectrum with characteristic sulfur peak (S) (red circle) resulting from CA and TG presence on the surface of the AuNPs.

with a slight band broadening after the addition of 1-thioglycerol (TG), while the peptide conjugation to particles surface shifted the absorption peak back to 522 nm. FT-IR spectra of TG and surface-modified AuNPs are similar, except for the absence of a 2582 cm^{-1} band of the −SH group, and slight shifting of some peaks in the modified particle absorption spectrum. The ammonium ions show a broad band at 2440 cm^{-1}, the absorption bands of amide I groups at 1735 cm^{-1} (C═O stretching vibration of peptide linkages), and the amide II groups around 1592 cm^{-1} (from a combination of N−H bending and C−N stretching), providing proof of the conjugation of peptide to the AuNP surface. FT-IR spectra interpretation is presented in Table S1 in Supporting Information. Characteristic peaks for carbon, oxygen, gold, copper,

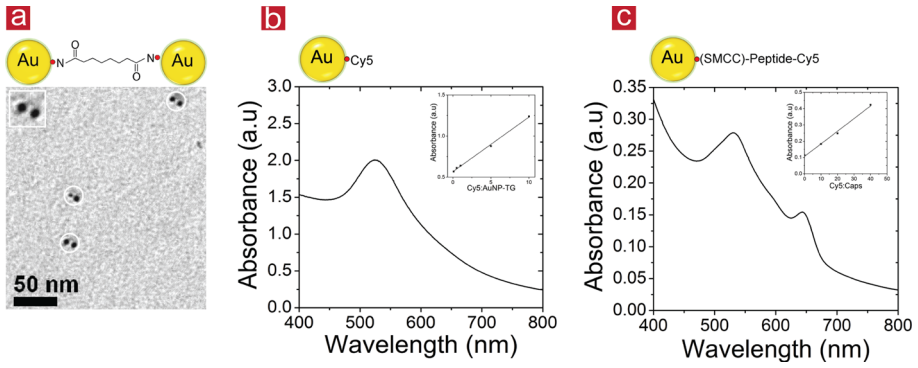

Figure 4. Validation of monofunctionality of AuNP used in the study, nanocluster Caps structure with surface peptide epitope. (a) TEM image of amide-coupling product of TG modified amine-AuNPs (carrying a single amino group of CA, *red ball*). The inset shows enlarged dimer with distance of ~2 nm. The corresponding schematic shows AuNP-dimer structure produced by the coupling reaction using DSS cross-linker, 62% of AuNP are in dimer form, meaning ~62% are monofunctional with a single amino group for subsequent steps. (b) Cy5-labeling of TG-modified amine-AuNPs (nonpeptide Caps). (c) Cy5-labeling of Caps (with peptide). The insets in panels a and b display standard curves prepared of known different molar ratios of Cy5 reacted with AuNPs-TG and Caps, respectively. The schematics represent the Cy5-labeled conjugates.

and sulfur were observed from the EDX spectrum. The corresponding elemental analysis table revealed a sulfur amount of 1.42%, indicating the presence of CA and TG (see Supporting Information, Table S2 for the exact amount of each element).

In addition to these techniques, amide coupling and Cy5 labeling reactions of TG-modified amine-AuNPs (free of peptide epitope) were designed to verify the monofunctionalized Au NPs carrying a single surface amino group of cysteamine available for peptide conjugation. Using disuccinimidyl suberate (DSS) cross-linker with two terminal NHS esters, AuNPs with a single surface amino group can be visualized when they self-couple to form AuNP-dimers (see schematic in Figure 4a). The incidence of AuNP-dimers is directly correlated to the monoaminofunctionality of coupled TG modified amine-AuNPs. The visualization of coupling reaction products, without purification, under TEM indicated the presence of ~62% of AuNPs-dimers (Figure 4a and Supporting Information, Methods).[20] The formation of dimer structures without multimer structure (multifunctionalized AuNP), with interdistance of ~2 nm, interestingly proves the surface stability of TG-AuNPs, which is highly significant for nanoclustering application in this report (see the inset of Figure 4a). Using Cy5-NHS ester to label amino groups of CA on AuNPs surface, the molar ratio of CA:TG-AuNPs was estimated to be 2.7 ± 1.43:1 as calculated from a standard curve prepared from known Cy5:TG-AuNPs molar ratios (Figure 4b and Supporting Methods), indirectly confirming the TEM dimerization assay data. Further Cy5 labeling of full structured Caps (with peptide) was applied to assess the number of functional peptide epitope per cap conjugate (see schematic in Figure 4c and Supporting Methods). The resulted Cy5 absorption spectrum confirmed the presence of ~1.39 ± 0.134 peptide per each Cap conjugate estimated from a standard curve, shown as an inset in Figure 4c. The total stability of the nanoparticles was monitored by observing the color change of the modified gold nanoparticles. The corresponding digital images in Figure 2 show insignificant color change in the resulting nanoparticle suspensions through the modification steps, confirming the stability of the particles. The total characterization analysis data prove the success of surface modification and peptide conjugation and assume the preparation of considerable percent of monofunctional Caps.

The core conjugates of multivalent Fab-QDs were prepared by Fab fragment coupling to the surface of QDs. The coupling was based on the efficient reaction of thiol groups (-SH) present in reduced Fabs with the maleimide groups present on the QD nanocrystals after SMCC activation (right panel of Figure 1 and Methods section). The efficiency of the coupling reaction was assessed by comparing the absorption and fluorescence spectra of core conjugates (Fab−QD) with those of unconjugated QDs dispersion. The results indicate that the absorption and emission spectra of Fab−QD Core are still symmetrical and almost identical to those of unconjugated QDs, with only a slight blue shift of emission maximum from 525 to 524.6 nm (Figure 5a,b). The number of Fabs per each core conjugate was quantified using bicinchoninic acid protein assay (BCA) as detailed in the Supporting Methods and each core conjugate was estimated to be covered by ~8 Fab molecules (Supporting Information, Figure S4). Agarose gel electrophoresis was used to evaluate the difference in the electrophoretic mobility after the coupling reaction (Figure 5c). The migration of QDs in gel is slightly retarded postconjugation, suggesting the addition of Fabs to their surface, which partially interferes with electrostatic behavior due to different size and charge density value between QDs and the Fab−QD conjugate (Core). In spite of the positive charge of $-NH_3^+$ on the surface of unconjugated QDs, it does not move to the cathode. This is due to the presence of PEG chains that make the

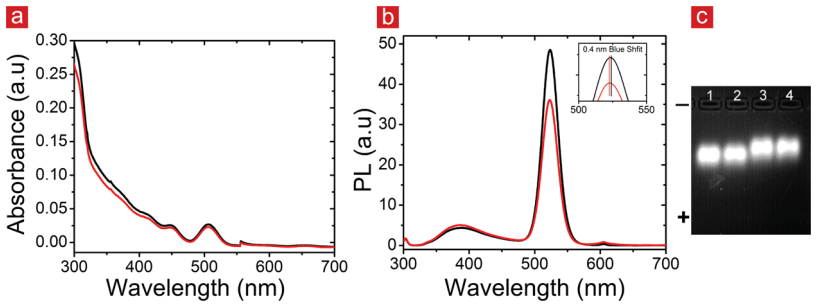

Figure 5. Nanocluster Core preparation and characterization. Optical characterization of Core in wavelength range of 700−300 nm: (a) UV−vis absorption spectra; (b) PL spectra of QDs (black) and Fab-QD Core (red) at 0.2 μM in 50 nM borate buffer (pH 8.5) by applying an excitation wavelength at 380 nm. The spectra reveal almost identical profiles before and after the conjugation step with only slight blue shift (0.4 nm) for peak PL spectrum of Core shown in the inset. (c) Gel electrophoresis of QDs (lane 1 and 2) and Fab−QD Core (lanes 3 and 4) show the difference in their electrophoretic mobility pattern. The different mobility indicates the successful conjugation of the Fab fragment onto the QD.

overall surface charge of nanoparticles slightly negative, allowing core nanoparticles to migrate toward the anode in the gel.[21] Furthermore, the enzyme-linked immunosorbent assay (ELISA) test was applied, to ensure the binding activity of Fabs after being coupled to QDs (Supporting Information, Figure S5).

In our interclustering approach, the preparation of cap acceptor conjugates monofunctionalized with a single peptide epitope is a key factor for quenching efficiency. By increasing the number of monofunctionalized acceptors (capping AuNP conjugates) around one donor (core QD conjugate), we can also produce discrete nanoclusters free of large aggregates, an issue faced by our peers when multifunctionalized acceptors were used, and cross-linking aggregates were common (Figure 6c,i and Supporting Information, Figure S6,i). AuNPs of 5.5 nm size were used, which lie in the size range of optimal Au quenchers (5−10 nm), as this small size was targeted to circumvent surface particle load limitation during the cluster assembly.[22] A short synthetic 13-aa peptide (~10 nm in full length) and its specific monoclonal antibody Fab fragments (~5 nm) were used to provide more compact acceptor and donor conjugates, producing a theoretical interclustering distance ≤16.5 nm (from center of QD to surface of AuNP, Supporting Information, Figure S7), which is smaller and more effective than the minimum effective energy transfer distance proposed for AuNPs as acceptors (up to 20 nm).[9] This distance is beyond the detection range for regular FRET, and much shorter than what is used in other reported plasmonic resonator immunological schemes, which makes it more advantageous than both FRET and previously reported NSET schemes. Antibody-Fabs are relatively smaller antigen-binding fragments with monovalent structure targeting a short epitomic peptide. The Fab fragments are anchored on the Core surface *via* the thiol group pre-existing at the hinge region of digested HBV preS2 antibody, so that the antigen recognition regions on Fab are oriented outward, and fully accessible to interact with acceptor capping conjugates or the

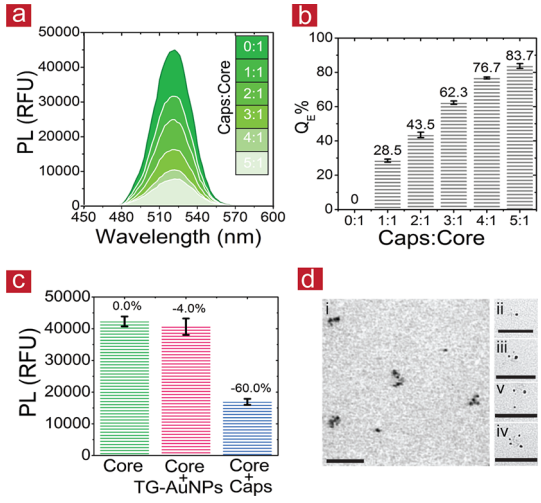

Figure 6. Nanocluster complex assembly. (a) Emission spectra of Core indicate the quenching responses to increasing Caps/Core ratio (0:1, 1:1, 2:1, 3:1, 4:1 and 5:1) where PL decrease, indicated by the diminishing of green color intensity with the increase in Caps/Core ratio. (b) Quenching efficiency (Q_E) as a function of Caps/Core ratio. (c) Fluorescence quenching response from same concentration of Core in the presence of 62 nM of TG-AuNPs (AuNPs free of peptide epitope, *Pink bar*) compared to 62 nM of Caps (AuNPs carrying peptide epitope, *Blue bar*) in 50 nM borate buffer pH 8.5. The corresponding percentages represent the calculated Q_E, and indicate insignificant quenching response in absence of specific peptide epitope. The concentration of Core was 20 nM. The Q_E was calculated following this equation; $Q_E = 1 - (PL_{Core\text{-}Cap}/PL_{core})$, where PL_{Core} is PL intensity of the Core alone, $PL_{Core\text{-}Caps}$ is PL intensity of Core in the presence of Cap(s). The error bars indicate the standard deviation in triplicate experiments. (d) TEM characterization of different nanocluster assemblies: (i) TEM shows the formation of distinctive clusters free from large aggregates; (ii−iv) TEM images of nanoclusters with different ratios of Caps (peptide-AuNPs, with higher contrast and larger in size) conjugated to Core (Fab-Qdot, with lower contrast and smaller in size) by Fab-epitope interaction (seen as a blurred shadow) 1:1, 1:2, 1:3, 1:4, respectively, scale bar = 100 nm.

competing HBV surface protein (right and central panel of Figure 1). The orientation of Fabs provides rapid specific interaction as a result of reduced steric hindrance and reduced nonspecific binding, all issues

commonly faced in large protein-antibody interactions.[23,24] QDs with green emission (525 nm) were chosen to produce a strong spectral overlap with the absorption band of AuNPs, which exhibit an absorption peak of 522 nm after peptide conjugation step (Figure 3b,i and Supporting Information, Figure S8). Thiol ligands of TG and PEG with pronounced ability to improve solubility and long-term stability of nanoparticles were used in our preparation scheme.[25,26]

Following this approach, an efficient nanocluster sensing platform was developed with several significant advantages and improvements, including (i) maximum quenching efficiency with a minimum quencher number for acceptor nanoparticles; (ii) improved energy transfer arising from the intrinsic quenching characteristic of AuNPs and by correlating the reporter detection signal to QDs photonic properties, which can be easily tuned with a minimal background interference;[22,27] (iii) flexible and rapid reconfiguration of cluster pattern (quenched to nonquenched) enabled by utilizing a molecular epitope-Fab interaction; (iv) maximum accessibility of donor conjugates afforded by the controlled orientation of Fab fragments on the surface of QDs; and (v) enhanced solubility and stability of cluster assemblies, following the use of TG and PEG polymer in the synthesis scheme.

To validate our proposed approach, we performed a fluorescence quenching assay, in which the same core conjugates concentration of Fabs−QDs was incubated, with an increasing capping conjugates ratio of peptide−AuNP conjugates to Fab−QD (Cap/Core =0:1, 1:1, 2:1, 3:1, 4:1, and 5:1). The collected QD photoluminescence (PL) spectra and the estimated quenching efficiency are shown in Figure 6a,b. A progressive decrease in PL, represented by the green curve, was observed as anticipated in a concentration-dependent manner with the increase of Cap/Core ratio. We found a remarkably enhanced quenching efficiency of 83% for a 5:1 molar ratio, as compared to the previous reports of Au−QDs based detection schemes, which were demonstrated at 83% for at best a 50:1 Au/QD ratio using 1.4 nm AuNPs.[9] In contrast, the addition of free gold nanoparticles (TG-modified amine-AuNPs without epitope) has a negligible quenching effect average of 4.0%. It is clear that even with a high concentration of unconjugated gold nanoparticles (62 nM), no significant fluorescence quenching happened, when compared to capping conjugates of peptide epitope−AuNPs (Figure 6c). The overall data establish the potential of our inter-nanoparticle clustering design to support an enhanced plasmonic quenching efficiency. Further investigation of the quenching assay products under TEM showed the formation of distinctive clusters free of large aggregates for preparations with Caps/Core molar ratios lower than 4:1 (Figure 6d,i Supporting Information, Figure S6,i). However, it was observed that the nanoclusters yielded consist of a heterogeneous population, with clusters of variable Caps/Core ratios. Figure 6d,ii−iv are representative TEM images of the assembled structures with different Caps/Core ratios (1:1−4:1), where the Caps, which have higher contrast and were larger in size, were conjugated to the Core, which has lower contrast and was smaller in size, by a Fab−epitope interaction seen as a blurred shadow bridge between Caps and Core (Figure S6, iii and v). An increase of Caps number over 4 molar excess to core conjugates was observed to result in a large clusters structure of core and cap conjugates (Figure S6,ii). The distance between QD and AuNPs in different nanoclusters was measured to be in the range of 25−8 nm, which is slightly more variable than the expected theoretical value (Supporting Information, Figure S7), that may be due to the preparation and imaging conditions required for TEM as previously reported to have high impact on bioassembled nanostructures.[28]

To explore the detection specificity of the preassembled cluster complex, we monitored the competitive dissociation of the cluster with the addition of specific and nonspecific protein, through a recovery response test. Bovine serum albumin (BSA) as a nonspecific protein was allowed to interact with the preassembled cluster complex, and the resulting recovery response was compared to that of the Hepatitis B surface antigen (HBsAg). The recovery response with BSA was insignificant compared to that of HBsAg, thus demonstrating a high sensing specificity (Supporting Information, Figure S9).

To obtain an insight into the detection sensitivity of our method, known concentrations of viral proteins of HBsAg (target antigen) and HCV Core antigen (HCVcoreAg, nontarget antigen as negative control) were incubated with the preassembled cluster complex (see Methods). The differences in PL intensities compared to the control (only buffer added) were calculated and plotted as a function of different concentrations of viral antigen (Figure 5a). The data show a progressive recovery of PL signal with increasing HBsAg concentration compared to HCVcoreAg. The detection limit of HBsAg is down to 0.1 pg/mL, which surpasses the current HBsAg detection limit of 0.15 ng/mL by at least 3 orders of magnitude.[29] The concentration-dependent PL recovery fitted curve exhibited a logarithmic behavior in the range extended from 0.1 to 0.0001 ng/mL, while the reaction became saturated as HBsAg concentration increased in range from 1 to 10 ng/mL[30] (Figure 7a and Supporting Information, Figure S10).

To further demonstrate the utility of the nanocluster in detecting real virus rather than recombinant proteins, Hepatitis B virus detection is tested to validate the feasibility of the NPR complex to detect and quantify HBV viral particles. Whole viral particles of

HBV (target) and HCV (nontarget control) were prepared using the HepG2-2.2.15 cell line and non-HBV-HCV infected serum, respectively (Supporting Information, Figures S11 and S12 and Methods). Different concentrations of target HBV viral particles (1, 5, 10, 50, 100, 500, and 1000 particles/μL) and nontarget HCV viral particles (10, 100, 500, and 1000 particle/μL) were incubated with aliquots of preassembled nanocluster complex, and the correlated PL recovery was determined. For HBV, the recorded recovery signals increased with elevated virus concentration, exhibiting an excellent linear correlation (Figure 7b) with a detection limit of one virus particle/μL, that is, nearly 50 virus particles per assay, for a sample volume of 50 μL; and a sensitivity of 100/μL. On the other hand, no significant recovery signals were recorded with HCV particles, proving specific sensing capability of nanoclusters (Figure 7b).

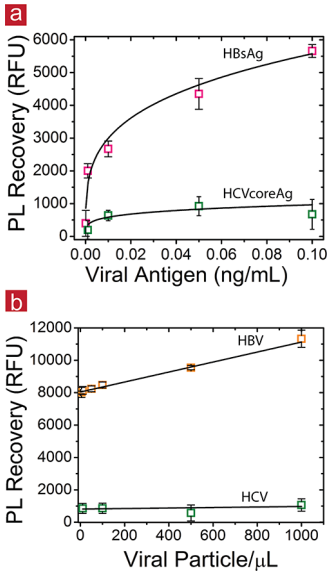

Figure 7. Nanocluster sensing action of HBV. (a) PL specific recovery response as a function of recombinant HBsAg protein (pink) concentration range (0.1−0.0001 ng/mL) and HCV Core protein (green) concentration range (0.1−0.001 ng/mL) plotted in the linear scale. (b) PL specific recovery response as a function of different HBV viral particle (orange) concentrations of 1, 10, 50, 100, 500, and 1000 particle/μL and HCV viral particle (green) concentrations of 10, 100, 500, and 1000 particle/μL plotted in the linear scale. The data were fit by nonlinear curve fit (Allometric1) for viral antigens and by linear curve fit for viral particle detection using Origin 8.5 software. Each data point is an average of three measurements, and error bars represent the standard deviation.

To investigate the kinetics of nanocluster sensing reaction, real time measurements of PL signals correlated to the assembly and disassembly interaction of its core and capping conjugates in the absence and the presence of competent HBsAg and HBV particles were recorded as indicated in the Methods section. PL signals resulting from mixtures of different Caps/Core molar ratios were measured for more than 2000 s to evaluate the binding assembly stability of the complex. The results of the time-dependent variations of PL signal with respect to different Caps/Core molar ratios are shown in Figure 8a. The transition and the equilibrium states for the Fab-coated core conjugates and the epitope-coated caps conjugates can be clearly distinguished. It was found that the binding process of the nanocluster core and caps conjugates led to a fast decrease of PL signal in the period from 100 to 250 s followed by an equilibrium in PL signal, which continues until more than 2000 s, demonstrating binding stability of the formed complex. The results also indicated that using higher ratios of caps conjugates caused a dramatic reduction of PL signal. Similarly, the kinetics of nanocluster complex disassembly caused by the addition of either HBsAg or HBV viral particles are depicted in Figure 8c,d. Aliquots of preassembled nanocluster complex were exposed to different concentrations of HBsAg (0, 0.01, and 0.1 ng/mL) or different concentrations of HBV particles (0, 100, and 1000 particle/μL) and the consequent disassembly action was monitored by measuring the PL signal for more than 800 s. The disassembly of nanocluster showed nearly a similar pattern in both cases of viral

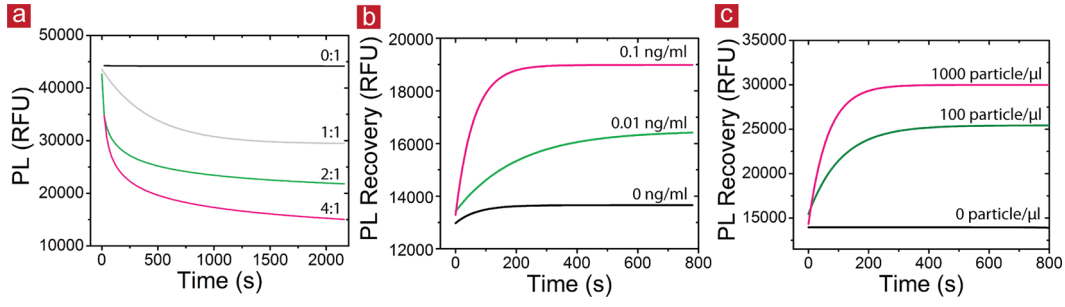

Figure 8. Nanocluster complex interaction kinetics. (a) Real time variation of PL quenching with assembly of different molar Caps/Core ratios of 0:1 (black), 1:1 (gray), 2:1 (green), and 4:1 (pink). (b) Real time variation of PL recovery with disassembly of preassembled NPR caused by the addition of different target HBsAg concentrations 0 (black), 0.01 (green), and 0.1 (pink) ng/mL. (c) Real time variation of PL recovery with disassembly of preassembled NPR caused by the addition of different HBV particle concentrations 0 (black), 100 (green), and 1000 (pink) particle/μL. The molar ratio of Core/Caps in preassembled NPR tested in panels b and c is 1:4. The presented graphs are fitting curves generated from the original data by nonlinear curve fit (exponential and logistic) using Origin 8.5 software.

surface antigen and complete viral particles (Figure 8c,d). Considering the sample preparation time, the signals began to release after the actual time of ~260 s after the addition of competent reactants due to the displacement of Caps (PL quencher) by either HBsAg or HBV particles, which have a slight unaccounted quenching effect on the Core PL signal. It was observed that the equilibrium state with HBsAg continued until 800 s, followed by a decrease in PL signal, indicating a possibility for a reassembly of nanocluster core and caps conjugates. In contrary, the PL signals in the case of viral particles interaction continued to be steady for more than 2000 s, which could be explained by the presence of excessive epitope copies on the surface of viral particles. Likewise, the addition of a higher concentration of HBsAg or HBV particles to the same concentration of preassembled nanocluster dramatically increased the PL signals.

CONCLUSION

Using our interclustering NPR complex approach, we developed an ultrasensitive, highly specific, and preassembled nanocomplex for fast detection of HBV particles and its surface antigen, using a new Core–Caps plasmonic nanocluster made of Fab–QD core–peptide epitope AuNP capping conjugate. This is one of the first instances of plasmonic detection of microorganisms with induced disassembly of gold–QDs nanocluster. We attribute the sensitivity to the enhanced energy transfer between luminescent QDs in the Core and AuNP plasmonic quenchers in the capping conjugates. Furthermore, multiple epitopes can be measured in microplate format, with full accessibility of highly specific molecular recognition elements of HBV monoclonal antibody Fab fragments. It is worth mentioning that our assay is a competitive assay, and achievement of high quenching efficiency using minimum capping conjugates decreases the detectable antigen concentration, which is critical for binding displacement reaction, and this in turn significantly affects the sensitivity of the assay. Additionally, the monofunctionalized peptide epitope–AuNP decreases the chance of large aggregates formation, which is quite frequent when using multifunctional acceptor conjugates. The disassembly reaction is more efficient and speedy due to the highly specific yet accessible epitope–antibody interaction. Rapid reconfiguration of the cluster pattern (from fluorescently quenched, preassembled nanocluster, to fluorescently nonquenched, disassembled nanocluster) using epitope–Fab binding affinity shortens the total test time frame to 30 min. We also successfully adopted the nanocluster to detect different concentrations of HBV viral particles, demonstrating its utility for early and fast detection without additional protein or nucleic acid sample preparation steps. The preassembled HBV NPR complex described here can also be applied for a broader use of microbial detection focusing on surface antigens, as well as multiplexed high-throughput assays in the future. Multiple epitopes can also be measured simultaneously to allow high-throughput serotyping, and for other pathogens.

METHODS

Preparation of Nanocluster Capping Conjugates. We used AuNPs (5.5 nm) for the preparation of monofunctionalized capping conjugates by coupling with the targeted peptide epitope. Citrate-capped AuNPs were synthesized by the reduction of chloroaurate ions of chloroauric acid hydrated ($AuCl_3 \cdot HCl \cdot 4H_2O$, Au $\geq$ 47.8%) by sodium borohydride ($NaBH_4$) in the presence of sodium citrate ($C_6H_5Na_3O_7 \cdot 2H_2O$). Monomaleimide functionalized gold nanoparticles were prepared from the synthesized AuNPs by a facile scheme, which was based on a sequential ligand exchange reaction in the presence of stabilizing nonionic surfactant Tween-20.[31,32] The surface of gold nanoparticles was first modified by the addition of cysteamine (CA) in a molar ratio of 1:1 to ensure one amino group for each particle, then 1- thioglycerol (TG) was allowed to assemble on the remaining surface area of the particles. Subsequently, the CA- and TG-stabilized gold nanoparticles were functionalized by SMCC, which interacts with the amino group (carried on CA) on the particle surface by its *N*-hydroxysuccinimide (NHS ester). A synthetic peptide epitope modified with C-terminal cysteine (13-aa in length, HQTLQDPRVRGLC) was synthesized. The peptide was allowed to couple through its terminal cysteine thiol group to the active maleimide group introduced to AuNPs surface by SMCC. The synthesized AuNPs particles and the prepared capping conjugates and their functional structure of peptide epitope were characterized by TEM, UV–vis, DLS, zeta potential, FT-IR, EDX, and Cy5 labeling absorption spectroscopy techniques. For detailed synthesis and characterization prescription, see the Supporting Methods.

Preparation of Nanocluster Core Conjugates. Fab fragments were generated from monoclonal antibody against HBV preS2 antigen (cat no. ab8635, Abcam) using Mouse IgG1 Fab and F(ab)2 Micro Preparation Kit (cat no. 44680, Pierce). Qdot 525 amine derivatized, PEG-coated nanocrystals were conjugated with the freshly prepared Fab fragments using Qdot 525 Antibody Conjugation Kit (cat no. Q22041MP, Invitrogen). The conjugation reaction was based on the efficient directional coupling of thiols that are present in reduced Fabs to the reactive maleimide groups present on the nanocrystals after SMCC activation. The synthesized core conjugates were characterized by optical characterizations and gel electrophoresis technique (Figure 5), and Fab fragments per core conjugate were quantified using bicinchoninic acid protein assay. The detailed steps are reported in the Supporting Methods.

Nanocluster Complex Assembly and Characterization. The cluster complex architecture was fabricated by combining capping and core conjugates. Their self-assembly is mediated *via* the specific interaction between the two nanoconjugates by epitope–Fabs interclustering elements (Figure 1). Complexes from different molar ratios of cap/core conjugates were prepared by mixing 5 μL of core conjugates (0.4 μM) and varying amounts of capping conjugates (1, 2, 3, 4, and 5 μL of 2 μM stock solution). Borate buffer (50 nM sodium tetraborate, pH 8.5) was added to adjust the final reaction volume to 100 μL, and then the mixtures were incubated in darkness for 15 min at room temperature. The morphology and particle structure of assembled complexes was investigated and characterized by TEM. The fluorescence quenching was assayed in Costar

96-well black opaque flat-bottomed plates (cat no. 3925, Corning) by measuring the fluorescence at an excitation wavelength of 380 nm using a microplate reader (Infinite M200, TECAN). Under the same conditions, the quenching efficiency of unconjugated gold (AuNPs free of peptides) was measured and compared to the same concentration, 62 nM, of Caps (AuNPs with peptides). The mean and standard deviation of the intensity were calculated from triplicate experiments. The relative quenching efficiency (Q_E) was determined by measuring the photoluminescence (PL) intensity of core conjugates in the presence and absence of capping conjugates.

Nanocluster Specificity and Sensitivity Assay. First, a working solution made of capping conjugates (80 nM) and Core (20 nM) was prepared in borate buffer and incubated in darkness for 15 min at room temperature. For detection of viral antigens, 50 μL aliquots of HBsAg dilutions (0.0001, 0.001, 0.01, 0.05, 0.1, 0.5, 1, 5, 10 ng/mL) and HCVcoreAg dilutions (0.001, 0.01, 0.05, 0.1 ng/mL) were prepared in borate buffer. To the control experiment wells, only borate buffer was added. Using the same experimental set up, the cluster complex detection specificity was confirmed by exposure to different concentrations of a nonspecific protein, BSA (0.001, 0.01, 0.05, 0.1, 0.5, and 1 ng/mL) side by side to the same concentrations of HBsAg as a specific protein. The PL signal intensity of each well was collected after 15 min of incubation. The signal (background corrected) was plotted as the difference between the fluorescence recorded for each viral antigen (HBsAg and HCVcoreAg) concentration and that collected from the control. All measurements were done in triplicate.

For detection of viral particles, Hepatitis B and C viral particles were prepared as indicated in the Supporting Information (Figure S11 and S12 and Supporting Methods). Aliquots (50 μL) of the previously described working solution were mixed with equal volumes (50 μL) of different viral particle dilutions (1−1000 particle/μL in borate buffer) in the wells of a microtiter plate. After incubation for 15 min in room temperature, the fluorescence signal was collected. The signal (background corrected) was plotted as the difference between the fluorescence recorded for each virus concentration (HBV and HCV) and that collected from the control (no virus). All measurements were done in triplicate.

Nanocluster Complex Interaction Kinetics. Both the assembly and disassembly responses of the nanocluster complex were evaluated using the previously mentioned microtiter plate-based experimental setup. To investigate the assembly interaction of nanocluster components of core and capping conjugates, 100 μL aliquots of different Caps/Core molar ratios (0:1, 1:1, 2:1 and 4:1) in borate buffer were allowed to assembly and the PL signal was measured. On the other hand, 50 μL aliquots of preassembled nanocluster prepared from a Caps/Core molar ratio of 4:1 were used to investigate the dissociation of a NPR nanocluster caused by the addition of 50 μL of different target HBsAg concentrations (0, 0.01, and 0.1 ng/mL) or HBV particles (0, 100, and 1000 particle/μL). The real time variations of the PL signal intensity were monitored for 15−30 min and plotted as a function of time. Data were fit by a nonlinear curve fit (exponential and logistic) using Origin 8.5 software.

Conflict of Interest: The authors declare no competing financial interest.

Acknowledgment. We thank J. Wo for discussions. The work was funded by Agilent Foundation Grant No. 09US-670, Zhejiang University International Student Fellowship, DOD Grant W81XWH-07-1-0663_BC061995, and U.S. DOE Contract DE-AC03-76SF00098.

Supporting Information Available: Detailed procedures and additional data of capping and core conjugates preparation and characterization. Preparation of Hepatitis B and C viral particles. Complete amino acid sequence of HBsAg/adw and the selected epitope containing peptide sequence. ELISA test to assess the Fab fragments activity after the core conjugates preparation. Experiments show PL recovery specificity to HBsAg compared to BSA and recorded PL recovery response as a function of HBsAg concentration range (10−0.05 ng/mL). TEM images show nanocluster assemblies. Additional schematics indicate the NPR intercluster distance theoretical model, spectral overlap of its capping and core conjugates, and the HBV particle isolation and purification. Tables include peak interpretation of IR spectra and EDX based elemental analysis of AuNPs surface modification products. This information is available free of charge *via* the Internet at http://pubs.acs.org.

REFERENCES AND NOTES

1. Mattei, G.; Mazzoldi, P.; Bernas, H., Metal Nanoclusters for Optical Properties. In *Materials Science with Ion Beams*; Bernas, H., Eds.; Springer: Berlin, 2009; pp 287−316.
2. Haglund, R. F., Nonlinear Optical Physics and Applications of the Plasmonic Response in Metal Nanoparticles. In *Photon-Based Nanoscience and Nanobiotechnology*; Tanev, S., Eds.; Springer: Quebec, 2006; pp 67−96.
3. Liu, G. L.; Kim, J.; Lu, Y.; Lee, L. P. Fluorescence Enhancement of Quantum Dots Enclosed in Au Nanopockets with Subwavelength Aperture. *Appl. Phys. Lett.* **2006**, *89*, 241118–241120.
4. Haridas, M.; Tripathi, L. N.; Basu, J. K. Photoluminescence Enhancement and Quenching in Metal-Semiconductor Quantum Dot Hybrid Arrays. *Appl. Phys. Lett.* **2011**, *98*, 063305–063308.
5. Govorov, A. O.; Bryant, G. W.; Zhang, W.; Skeini, T.; Lee, J.; Kotov, N. A.; Slocik, J. M.; Naik, R. R. Exciton-Plasmon Interaction and Hybrid Excitons in Semiconductor-Metal Nanoparticle Assemblies. *Nano Lett.* **2006**, *6*, 984–994.
6. Li, X. Q.; Ratchford, D.; Shafiei, F.; Kim, S.; Gray, S. K. Manipulating Coupling between a Single Semiconductor Quantum Dot and Single Gold Nanoparticle. *Nano Lett.* **2011**, *11*, 1049–1054.
7. Wang, X.; Guo, X. Q. Ultrasensitive Pb(2+) Detection Based on Fluorescence Resonance Energy Transfer (FRET) between Quantum Dots and Gold Nanoparticles. *Analyst* **2009**, *134*, 1348–1354.
8. Liu, H.; Liang, G.; Abdel-Halim, E. S.; Zhu, J.-J. A Sensitive and Selective Quantum Dots-Based FRET Biosensor for the Detection of Cancer Marker Type IV Collagenase. *Anal. Methods* **2011**, *3*, 1797–1801.
9. Kim, H. S.; Kim, Y. P.; Oh, Y. H.; Oh, E.; Ko, S.; Han, M. K. Energy Transfer-Based Multiplexed Assay of Proteases by Using Gold Nanoparticle and Quantum Dot Conjugates on a Surface. *Anal. Chem.* **2008**, *80*, 4634–4641.
10. Tang, B.; Cao, L. H.; Xu, K. H.; Zhuo, L. H.; Ge, J. H.; Li, Q. F.; Yu, L. J. A New Nanobiosensor for Glucose with High Sensitivity and Selectivity in Serum Based on Fluorescence Resonance Energy Transfer (FRET) between CdTe Quantum Dots and an Nanoparticles. *Chem.—Eur. J.* **2008**, *14*, 3637–3644.
11. Li, X.; Qian, J.; Jiang, L.; He, S. L. Fluorescence Quenching of Quantum Dots by Gold Nanorods and Its Application to DNA Detection. *Appl. Phys. Lett.* **2009**, *94*, 063111–063114.
12. Lu, Y.; Liu, J. W.; Lee, J. H. Quantum Dot Encoding of Aptamer-Linked Nanostructures for One-Pot Simultaneous Detection of Multiple Analytes. *Anal. Chem.* **2007**, *79*, 4120–4125.
13. Kim, H. S.; Kim, Y. P.; Park, S.; Oh, E.; Oh, Y. H. On-Chip Detection of Protein Glycosylation Based on Energy Transfer between Nanoparticles. *Biosens. Bioelectron.* **2009**, *24*, 1189–1194.
14. Kim, H. S.; Oh, E.; Lee, D.; Kim, Y. P.; Cha, S. Y.; Oh, D. B.; Kang, H. A.; Kim, J. Nanoparticle-Based Energy Transfer for Rapid and Simple Detection of Protein Glycosylation. *Angew. Chem., Int. Ed.* **2006**, *45*, 7959–7963.
15. Huang, C. Z.; Hu, P. P.; Chen, L. Q.; Liu, C.; Zhen, S. J.; Xiao, S. J.; Peng, L.; Li, Y. F. Ultra-sensitive Detection of Prion Protein with a Long Range Resonance Energy Transfer Strategy. *Chem. Commun.* **2010**, *46*, 8285–8287.
16. Ray, P. C.; Darbha, G. K.; Ray, A. Gold Nanoparticle-Based Miniaturized Nanomaterial Surface Energy Transfer Probe for Rapid and Ultrasensitive Detection of Mercury in Soil, Water, and Fish. *ACS Nano* **2007**, *1*, 208–214.
17. Schasfoort, R. B. M., Tudos, A. J., Eds. *Handbook of Surface Plasmon Resonance*; RSC Pub.: Cambridge, UK, 2008; 403 p.

18. Ray, P. C.; Fortner, A.; Darbha, G. K. Gold Nanoparticle Based FRET Assay for the Detection of DNA Cleavage. *J. Phys. Chem. B* **2006**, *110*, 20745–8.
19. Ray, P. C.; Darbha, G. K.; Ray, A.; Hardy, W.; Walker, J. A Gold-Nanoparticle-Based Fluorescence Resonance Energy Transfer Probe for Multiplexed Hybridization Detection: Accurate Identification of Bio-Agents DNA. *Nanotechnology* **2007**, *18*, 375504–375506.
20. Shaffer, A. W.; Worden, J. G.; Huo, Q. Comparison Study of the Solution Phase *versus* Solid Phase Place Exchange Reactions in the Controlled Functionalization of Gold Nanoparticles. *Langmuir* **2004**, *20*, 8343–8351.
21. Bernardin, A.; Cazet, A.; Guyon, L.; Delannoy, P.; Vinet, F.; Bonnaffe, D.; Texier, I. Copper-Free Click Chemistry for Highly Luminescent Quantum Dot Conjugates: Application to *in Vivo* Metabolic Imaging. *Bioconjugate Chem.* **2010**, *21*, 583–588.
22. Krull, U. J.; Algar, W. R.; Massey, M. The Application of Quantum Dots, Gold Nanoparticles, and Molecular Switches to Optical Nucleic-Acid Diagnostics. *Trac-Trend Anal. Chem.* **2009**, *28*, 292–306.
23. Barboni, E. A. M.; Bawumia, S.; Hughes, R. C. Kinetic Measurements of Binding of Galectin 3 to a Laminin Substratum. *Glycoconj. J.* **1999**, *16*, 365–373.
24. Beale, D. Molecular Fragmentation—Some Applications in Immunology. *Dev. Comp. Immunol.* **1987**, *11*, 287–296.
25. O'Brien, P.; Berhanu, D.; Govender, K.; Smyth-Boyle, D.; Archbold, M.; Halliday, D. P. A Novel Soft Hydrothermal (SHY) Route to Crystalline PbS and CdS Nanoparticles Exhibiting Diverse Morphologies. *Chem. Commun.* **2006**, *45*, 4709–4711.
26. Duan, H. W.; Nie, S. M. Cell-Penetrating Quantum Dots Based on Multivalent and Endosome-Disrupting Surface Coatings. *J. Am. Chem. Soc.* **2007**, *129*, 3333–3338.
27. Jo, W. H.; Hong, S. H.; Hong, S. W. A New Polymeric pH Sensor Based on Photophysical Property of Gold Nanoparticle and pH Sensitivity of Poly(sulfadimethoxine methacrylate). *Macromol. Chem. Phys.* **2010**, *211*, 1054–1060.
28. Wang, Q. B.; Wang, H. N.; Lin, C. X.; Sharma, J.; Zou, S. L.; Liu, Y. Photonic Interaction between Quantum Dots and Gold Nanoparticles in Discrete Nanostructures through DNA Directed Self-Assembly. *Chem. Commun.* **2010**, *46*, 240–242.
29. Weber, B. Recent Developments in the Diagnosis and Monitoring of HBV Infection and Role of the Genetic Variability of the S Gene. *Expert. Rev. Mol. Diagn.* **2005**, *5*, 75–91.
30. Dai, H. J.; Chen, Z.; Tabakman, S. M.; Goodwin, A. P.; Kattah, M. G.; Daranciang, D.; Wang, X. R.; Zhang, G. Y.; Li, X. L.; Liu, Z.; *et al*. Protein Microarrays with Carbon Nanotubes as Multicolor Raman Labels. *Nat. Biotechnol.* **2008**, *26*, 1285–1292.
31. Feldheim, D. L.; Liu, Y. L.; Shipton, M. K.; Ryan, J.; Kaufman, E. D.; Franzen, S. Synthesis, Stability, and Cellular Internalization of Gold Nanoparticles Containing Mixed Peptide−Poly(ethylene glycol) Monolayers. *Anal. Chem.* **2007**, *79*, 2221–2229.
32. Aslan, K.; Perez-Luna, V. H. Surface Modification of Colloidal Gold by Chemisorption of Alkanethiols in the Presence of a Nonionic Surfactant. *Langmuir* **2002**, *18*, 6059–6065.